JOURNAL OF MATERIALS SCIENCE **34** (1999) 1573–1582

Influences of Fe-impurity on the production process of SiC fiber reinforced Al for electric cables

Y. YASUTOMI
Japan Fine Ceramics Center, 2-4-1, Mutsuno, Atsuta-ku, Nagoya, 456-8587 Japan
E-mail: yasutomi@purple.plala.or.jp

J. SAWADA, T. KIKUCHI
Tokyo Electric Power Co., 4-1, Egasaki-cho, Tsurumi-ku, Yokohama, 230-8510 Japan

K. NAKAMURA, Y. MANABE
Chubu Electric Power Co., 1, Toshin-cho, Higashi-ku, Nagoya, 461-8680 Japan

K. NAGANO, H. KURODA, T. SUMI, H. KUBOKAWA, M. NAGAI, H. KOGURE
Power System Laboratory, Hitachi Cable, Ltd., 4-10-1, Kawajiri-cho, Hitachi, 319-1411 Japan

Y. SAWAI
Hitachi Research Laboratory, Hitachi, Ltd., 7-1-1, Omika-cho, Hitachi, 319-1292 Japan

T. KISHI
RCAST, University of Tokyo, 4-6-1, Komaba, Meguro-ku, Tokyo, 153-0041 Japan

As electrical power demands increase every year, the need becomes stronger for light weight electric cables which have high transmission capacity, high thermal resistance and low sag. We have developed a SiC fiber reinforced aluminum electrical cable to meet this need. Mechanical properties of the SiC/Al composite conductor are very susceptible to iron impurity which becomes mixed in the Al matrix during manufacture of the composite conductor. In this work, we studied the effects of Fe impurity in Al on fracture behavior of the composite conductor. A preformed wire was prepared by dipping a bundle of 1500 pieces of SiC fiber (Si: 63.7, C: 35.8, O: 12.3 mass %) into molten Al in which 0.36 mass % Fe and 0.5 mass % Ti were mixed. The Ti was added to improve the wetting property. Test samples were prepared by bundling seven preformed wires together. A tensile test was carried out for the composite conductor, and pull-out behavior of SiC fiber at the fracture surface was observed by scanning electron microscopy (SEM), energy dispersive X-ray spectroscopy (EDX) and electron probe micro analysis (EPMA). Pull-out of SiC fiber was observed at the fracture surface of the composite conductor using Fe-free Al. However, pull-out of SiC fiber was not observed at the fracture surface of the composite conductor using Fe-containing Al since Al was combined inseparably with the SiC and Fe. The fracture origin of the Fe-containing sample was a precipitated Fe-compound at the SiC/Al interface. Tensile strength of the Fe-containing sample was a half of that of the Fe-free sample. We propose the following the precipitation mechanism for the Fe compound. In manufacturing of the preformed wire, molten Al solidifies from the surface to the SiC/Al interface because of the low thermal conductivity of the SiC fiber. In the cooling process, Fe-free Ti-compound precipitates in the molten Al by a peritectic reaction. This leads to a higher concentration of Fe in the molten Al near the interface, and finally, $FeAl_3$ compound precipitates at the SiC/Al interface.

1. Introduction

As more electric power is demanded every year, it becomes necessary to increase the carrying capacity. But constructing more electric power transmission towers in large cities which have no more vacant space is not possible, so alternative means must be considered. The temperature limit of recently developed conductors, such as ultra thermo-resistant Al alloy conductors with steel reinforcing (UTACSR) and extra thermo-resistant aluminum alloy conductors with aluminum-clad invar reinforcing (XTACIR), is 200 °C owing to their thermal expansion properties. To double the carrying capacity of the present thermo-resistant Al power cable using such conductors, a thicker power cable is necessary

to decrease the Joule heat generation. The increase in weight requires that cable transmission towers be strengthened. Thus lightweight electric cables which have high transmission capacity, high thermal resistance and low sag, has been the object of joint research by the Tokyo Electric Power Co., Chubu Electric Power Co. and Hitachi Cable, Ltd. [1, 2].

Studies on SiC/Al composites cable by TEM confirmed that there is no reactant at the SiC/Al interface [3, 4]. Other groups have studied mechanical properties of SiC fiber/Al composites [5–12]. It has been feared that the quality of the SiC/Al power cable is deteriorated by the SiC/Al interface reaction. Ordinarily, Al becomes mixed with Fe impurity in the manufacturing process and few reports have studied the influence of Fe impurities on the strength of SiC fiber reinforced Al composite. Mechanical properties of the SiC/Al composite conductor are very susceptible to Fe impurity which is mixed in the Al matrix during the conductor manufacture. In this work, we studied effects of Fe impurity in Al on fracture behavior of the composite conductor.

2. Experimental procedure

2.1. Production of SiC fiber/Al composite cable

Production of the SiC fiber (Si: 63.7, C: 35.8, O: 12.3 mass %)/Al composite cable is described in Fig. 1. The SiC fiber is polycarbosilane fiber, which was oxidation-cured at 1200 to 1500 °C. It consists of β-SiC particles about 3 to 5 nm in diameter and containing 12% oxygen. Fifteen hundred pieces of fiber(10 μm diameter) with lengths from 500 to 1000 m make up one bundle. SiC/Al preformed wire is prepared by dipping this SiC fiber bundle into molten Al (JIS standard A-1050) at 700 °C and reeling it continuously. Titanium (0.5 mass %) is added to the molten Al to improve the wettability with SiC fiber. To confirm the effects of Fe impurity on mechanical properties of the composite cable, molten Al containing 0.36 mass % Fe is used. The preformed wire has a circular cross section with a diameter of 0.5 mm. Al is well distributed among the SiC fibers. The volume fraction of the fiber is 40%. Dipped SiC fiber/Al wire with a diameter of 2.6 mm is prepared by bundling seven preformed wires together and dipping them into the molten Al, passing the new bundle through a solid die, and then rolling. The SiC fiber/Al elemental wire, with a diameter of 3.2 mm and 17.8% volume fraction of fiber, is obtained by covering the dipped wire with Al in an extrusion process. Fe-free SiC/Al elemental wire is denoted as high strength elemental wire, and Fe mixed SiC/Al elemental wire is low strength elemental wire. Electric cable for practical use is produced by bundling 37 elemental wires of SiC fiber/Al composite elemental wire.

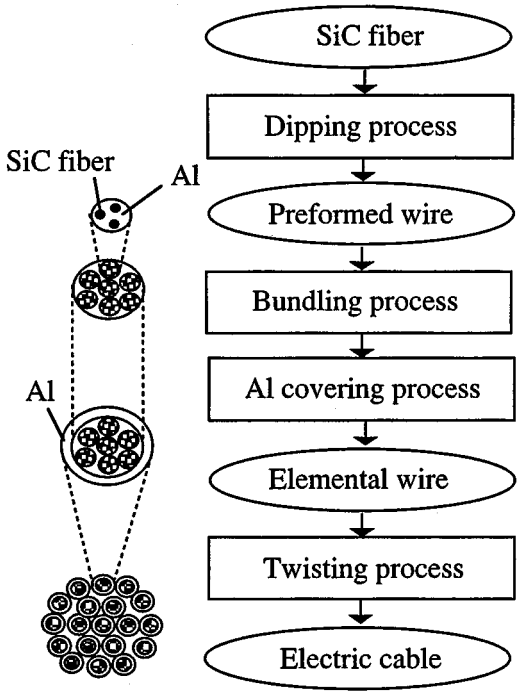

Figure 1 Production flow chart for SiC fiber reinforced aluminum composite electric cable.

2.2. Analytical methods

The composite elemental wire samples were cut from longer wires into 180 mm lengths, and tensile strength was examined with a tensile testing machine (Shimazu Autograph AG5000C). Pull out of the fiber at the fracture surface was observed with an SEM (Hitachi S-800). The fracture origin of SiC fiber was analyzed using SEM and EDX (Gatan) methods. A polished cross section of the composite elemental wire was analyzed with an EPMA (Perkin Elmer PHI-670) under the following conditions: 15 kV = acceleration voltage; 15 μA = current; 1 μm = spot size; 50 ms/point = scan speed. Each sample was analyzed with a transmission electron microscopy (TEM) (Hitachi, H-9000NAR; 300 kV). EDX (Gatan) analysis was also carried out to get details.

2.3. Observation of fracture process

Fracture behavior of samples for the *in situ* 3-point bending tests was observed by SEM (Fig. 2). A special test machine (Instron Japan Co.) was installed in the SEM chamber (Hitachi S-570). The bending rate was 0.005 mm/s. The test machine was stopped when SEM photos were taken. A video tape recording of the fracture behavior was also made from the microscope images.

2.4. Measurement of radius of curvature of the elemental wire at the point of interface exfoliation

Bonding behavior of SiC fiber and Al of each composite elemental wire can be compared by studying exfoliation behavior of the SiC fiber/Al interface. To compare the bonding behavior, curvature of the test sample at the point of exfoliation was measured.

3. Results and discussion

3.1. Tensile strength properties

Tensile strengths of high and low strength elemental wires are 390 and 190 MPa, respectively. Fig. 3 shows

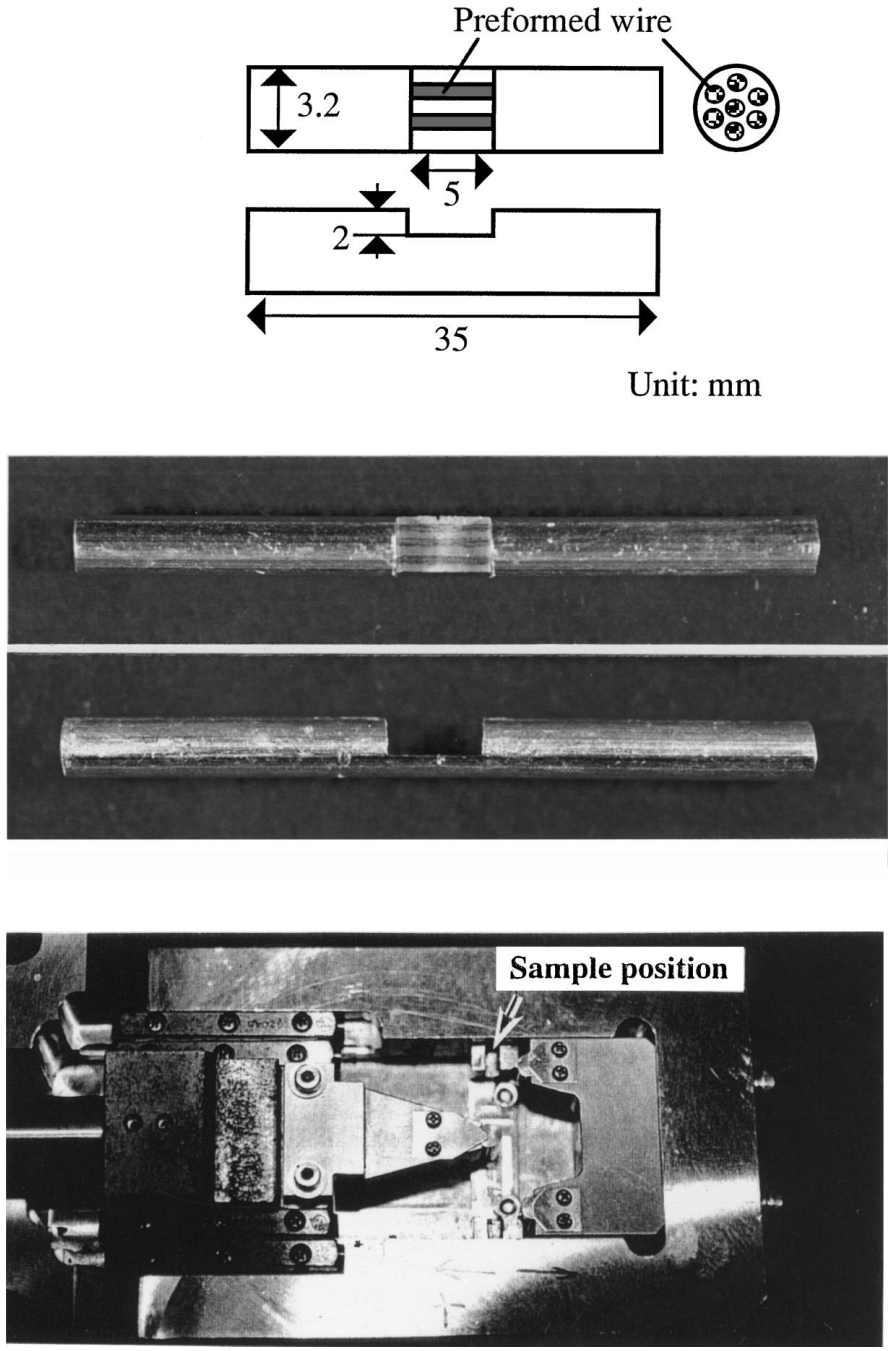

Figure 2 Testing sample and special testing machine for in-situ fracture behavior observation.

SEM images of the tensile fracture surface of the two wires. Unevenness of the fracture surface of the high strength elemental wire is larger than that of the low strength elemental wire, and elongation of the Al matrix is also larger for the former. Pull-out of preformed wire and SiC fiber is observed at the fracture surface of the high strength elemental wire, but not for the low strength one. Thus the SiC fiber/Al interface of the low strength elemental wire holds more strongly than that of the high strength one.

Fig. 4 shows the load-elongation diagram of the two elemental wires. Slopes of both curves in the elasticity area are similar, indicating that the elasticity coefficients of both samples are almost the same. Therefore, elongation of low strength elemental wire at the point of fracture is smaller than that of high strength elemental wire.

SEM observations of the fracture surface after tensile tests were made and Fig. 5 shows SEM micro graphs of fracture surface and the fracture origin of SiC fiber. No Fe compound is detected at the fracture origin of fiber of the high strength elemental wire. On the other hand, it is readily detected there for the low strength elemental wire.

3.2. Fracture process

To observe the pull-out behavior of SiC fiber, (1) *in situ* SEM observations of 3-point bending tests and (2) video tape recordings of 3-point bending tests when using a fiber scope were carried out. Fig. 6 shows SEM images of high and low strength elemental wires at the early stage of fracture, the middle stages, and the final stage. Unevenness of cracking is intense in the

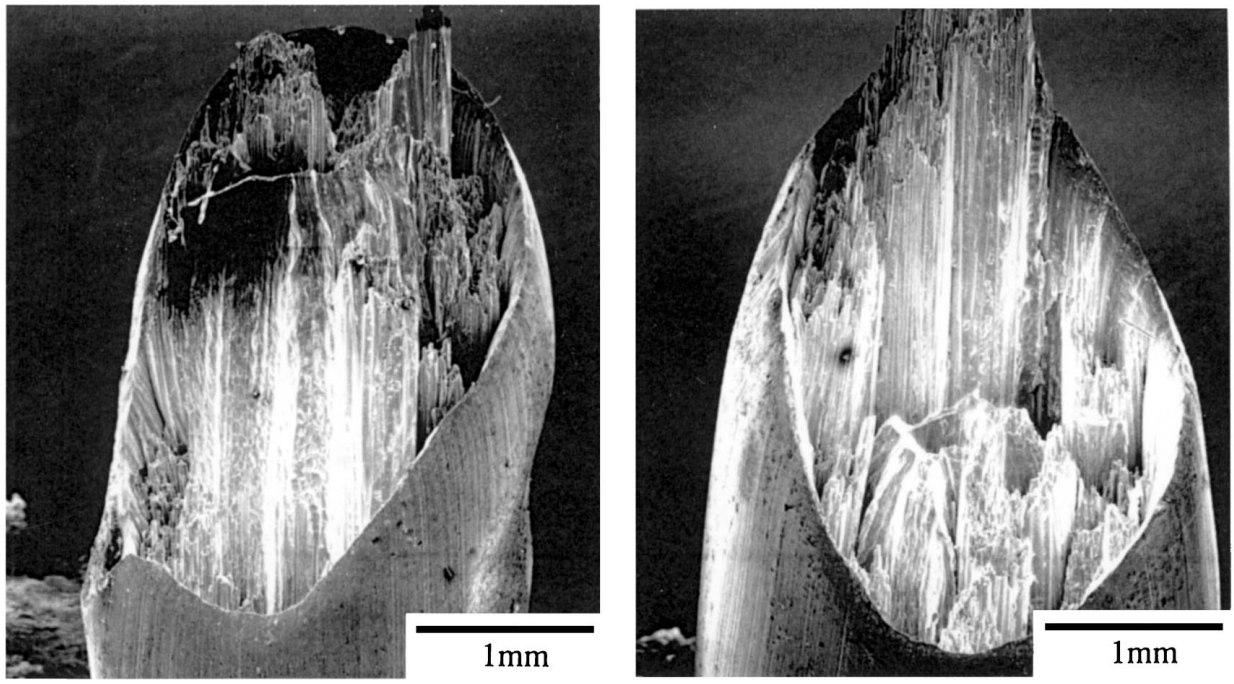

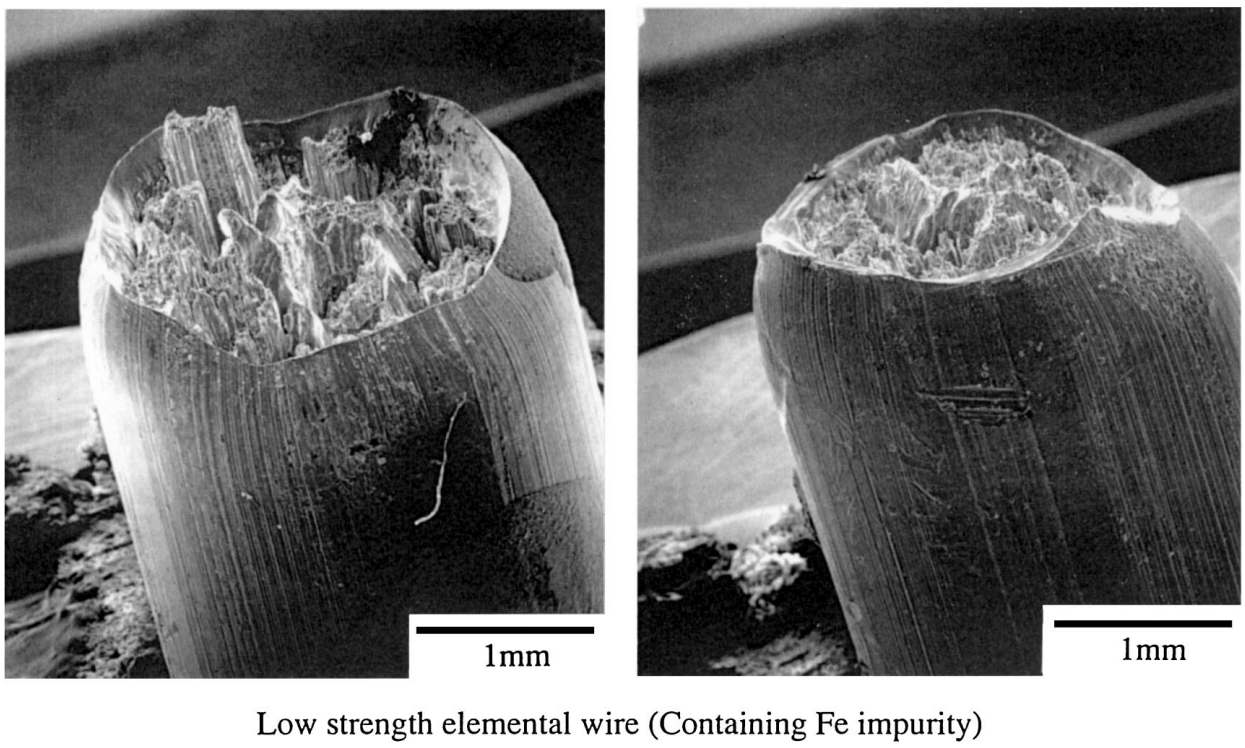

Figure 3 SEM images of tensile fracture surfaces of elemental wires.

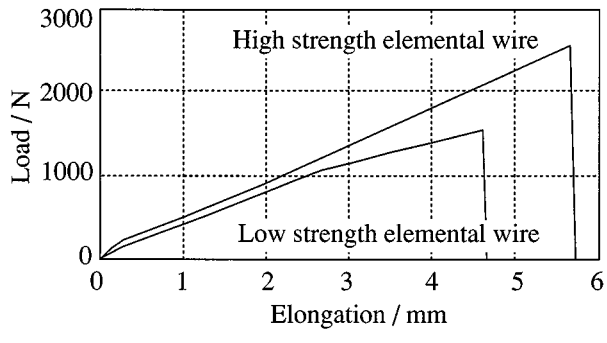

Figure 4 Load-elongation diagram of the two elemental wires.

fracture area of high strength elemental wire indicating that a slippage occurs at the SiC fiber/Al interface, and pull-out results. On the other hand, unevenness of cracking in the low strength elemental wire is gradual, indicating that no slippage occurs at its interface. Slippage is prevented by the presence of Fe compounds at the interface of the sample, and sample destruction occurs without fiber pull-out.

Video tape recordings of the fracture process were studied next. In Fig. 7, letter A denotes the covered Al part; B, the outer Al part of the dipping wire, C, preformed wire; D, the inner Al part of the dipping

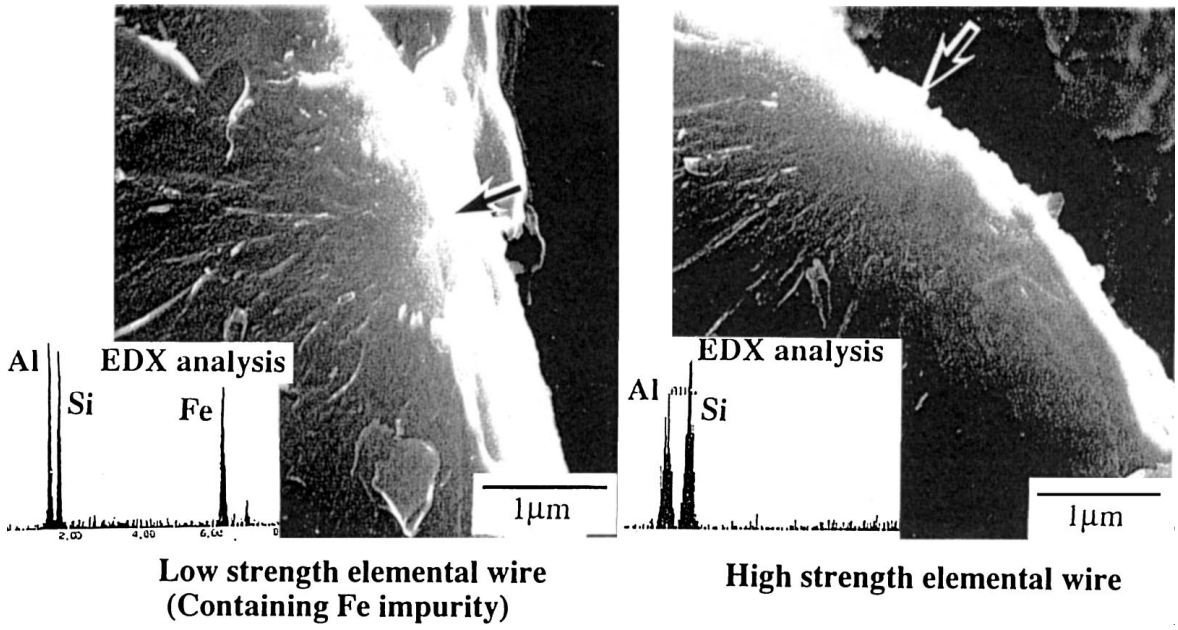

Figure 5 Fracture origin of SiC fibers.

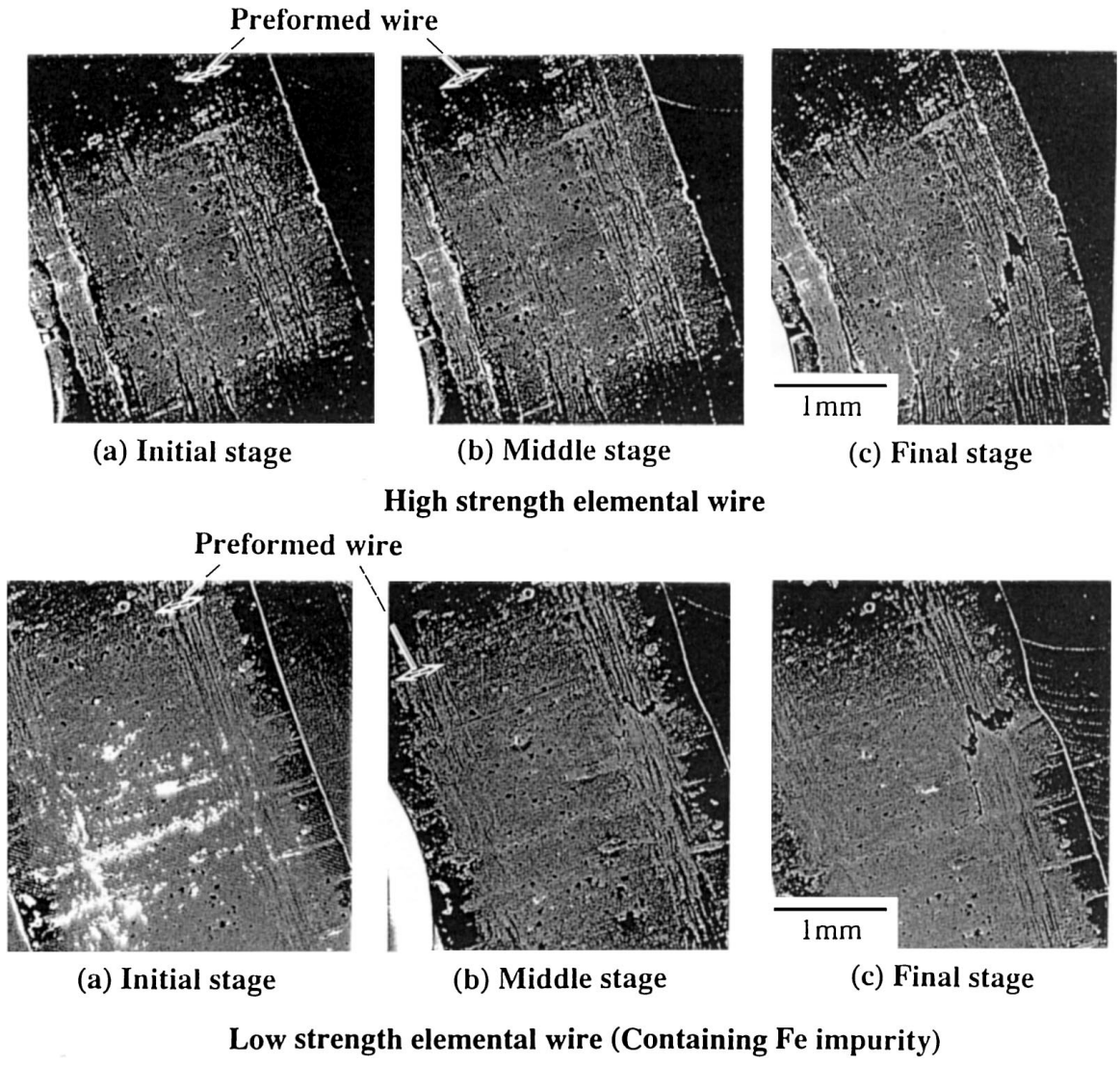

Figure 6 Fracture process of elemental wires by *in situ* SEM observation of 3-point bending test.

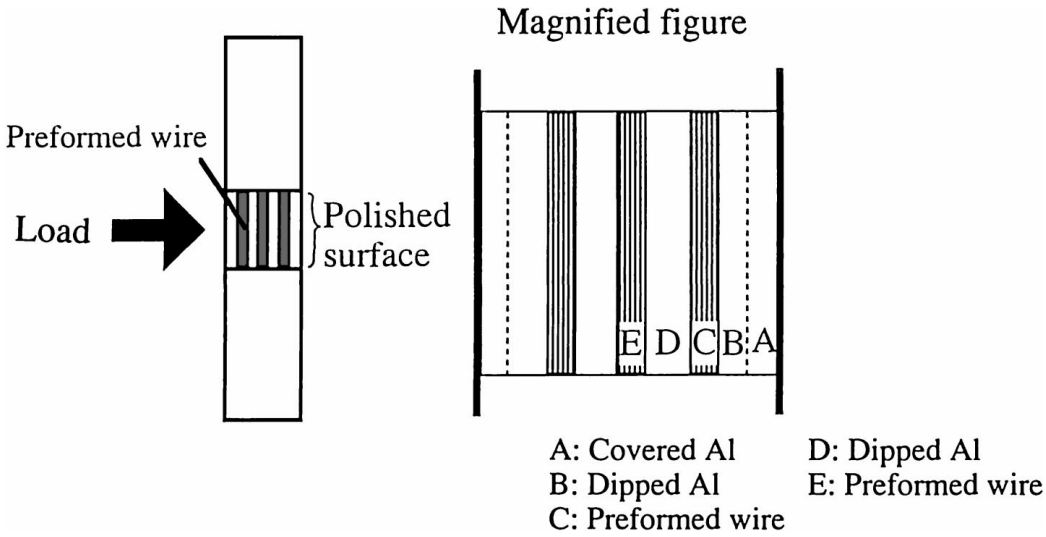

Figure 7 Schematic of test sample for fracture behavior observation.

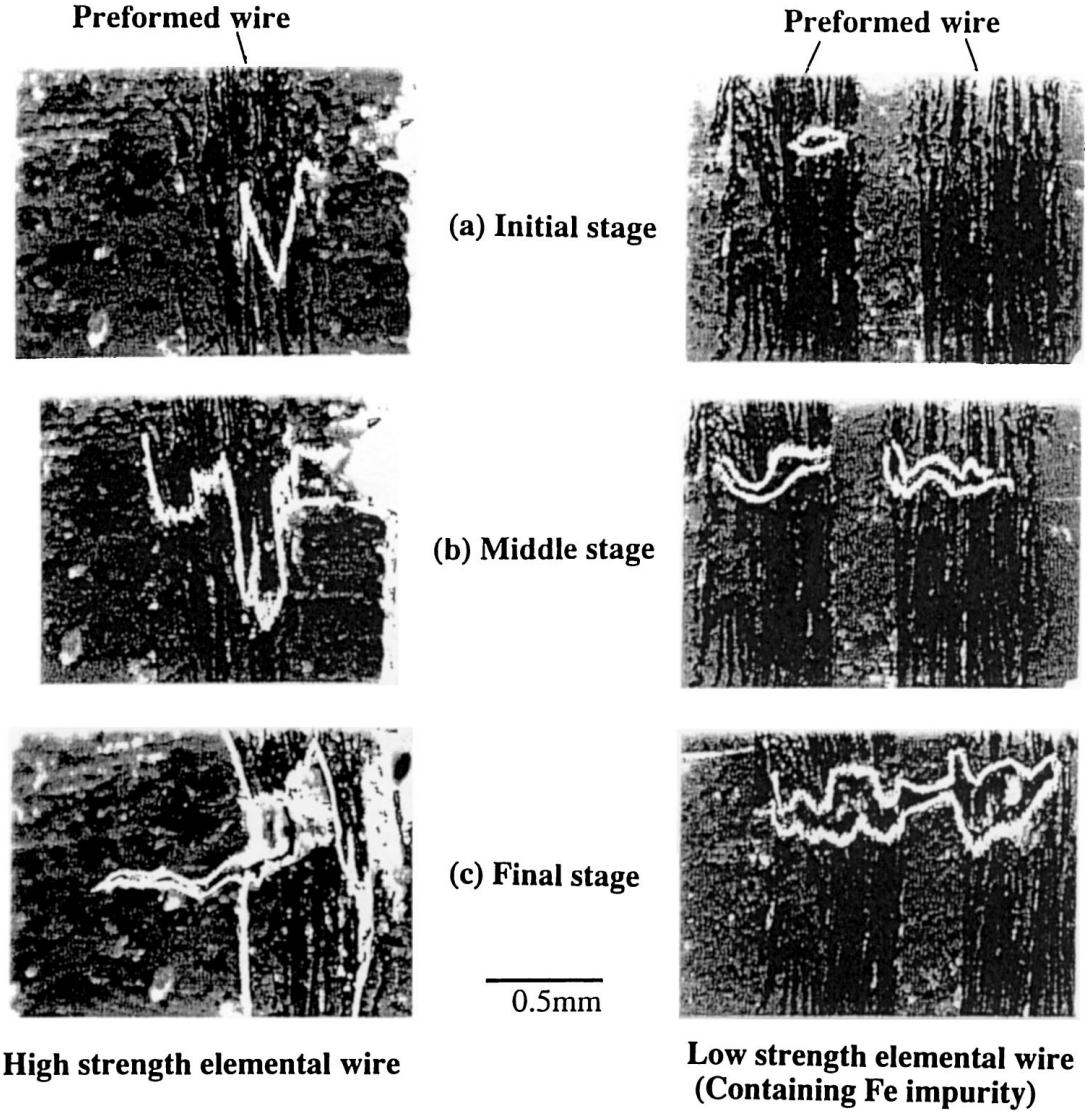

Figure 8 In situ video tape recorded pictures of 3-point bending tests of elemental wires.

wire; and E, preformed wire. During 3-point bending tests, the high strength elemental wire is demanded. The fracture process is explained from Fig. 8 as follows.

(1) The A/B interface is exfoliated.

(2) A break occurs across the preformed wire C (Fig. 8a).

(3) A break occurs across B (Fig. 8b).

(4) A break occurs across another preformed wire E.

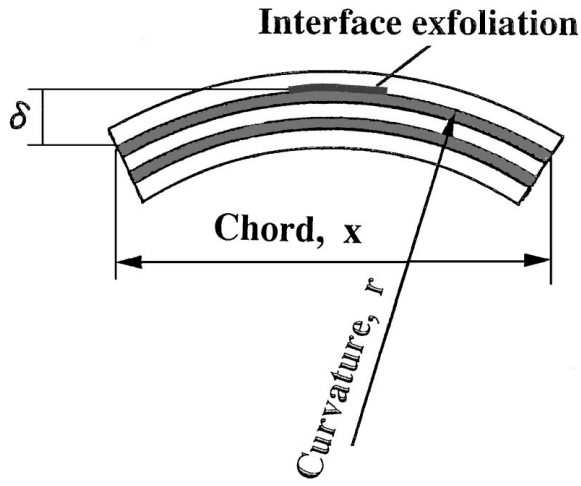

Figure 9 Radius of curvature of the composite wire at the point of interface exfoliation.

(5) A break occurs across A.
(6) A break occurs across the dipped Al region D.

The sample breaks in the order C, B, E, A, D, and we believe that the extent of A breaking is independent of the extent of E breaking.

Fig. 8 also shows typical video images from the fracture process of the low strength elemental wire. This wire breaks in the same order as the high strength one. Unevenness at the fracture surface of the high strength elemental wire is larger than that of the low strength elemental wire, and the fracture surface of the low strength elemental wire is flat. In both cases, the unit material breaking in regions C and E is not SiC fiber, but the preformed wire. Tensile stress at the Al matrix for dipped composite wire is lower than that of coating Al, nevertheless the Al of dipping composite is broken earlier than the coating Al.

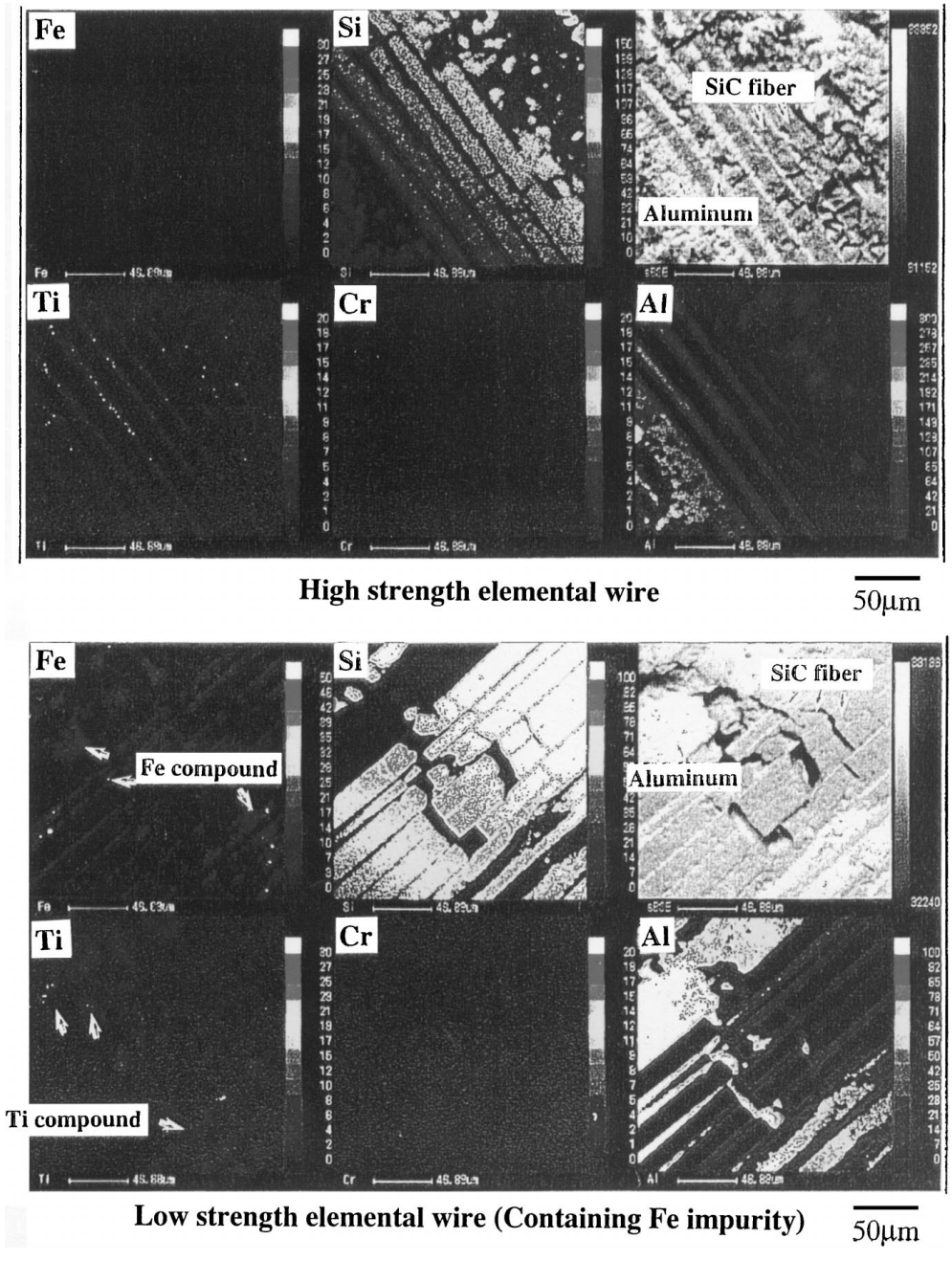

Figure 10 EPMA analyses of crack propagation area of elemental wires.

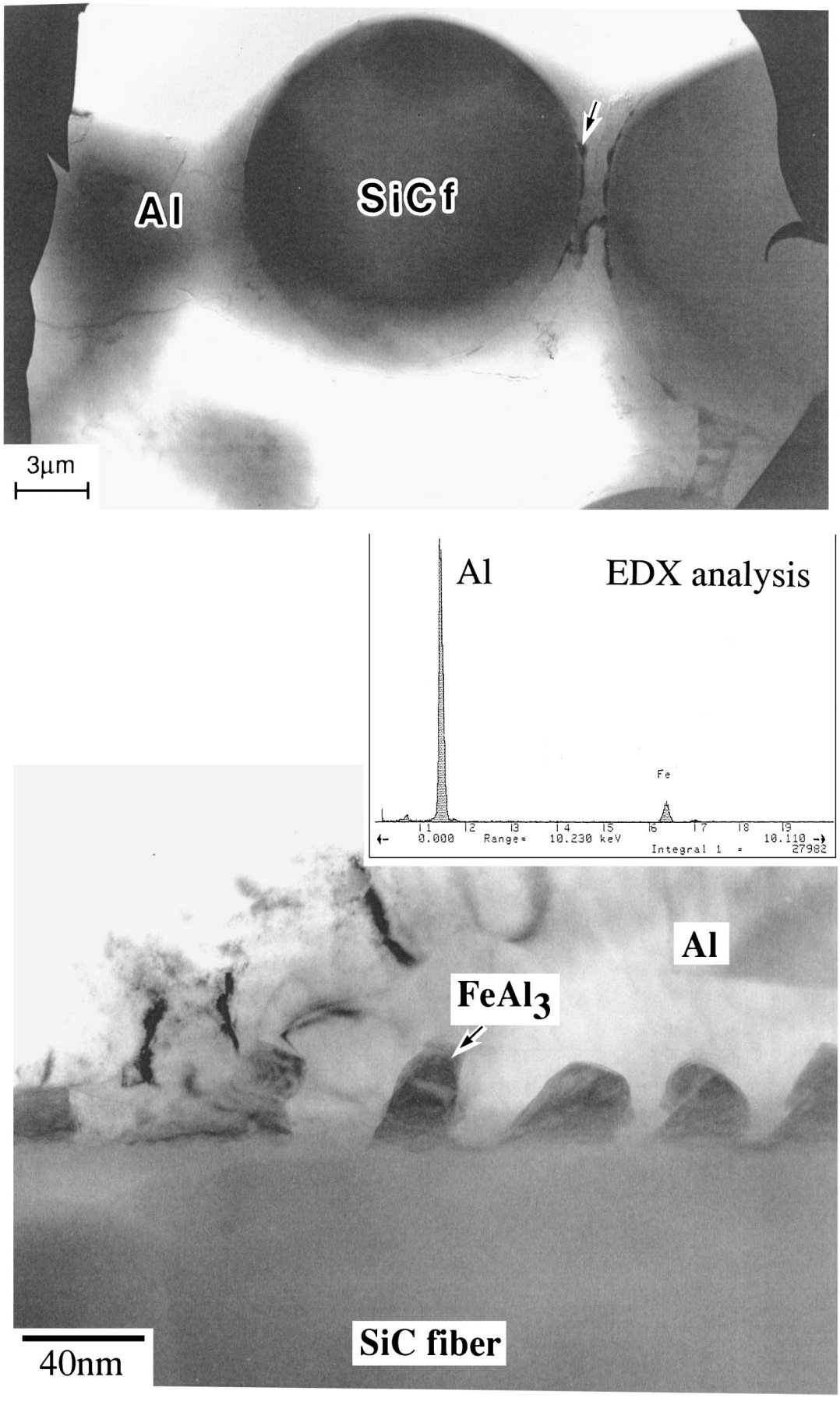

Figure 11 TEM images and EDX analysis of $FeAl_3$ compound in the SiC/Al interface of low strength elemental wire.

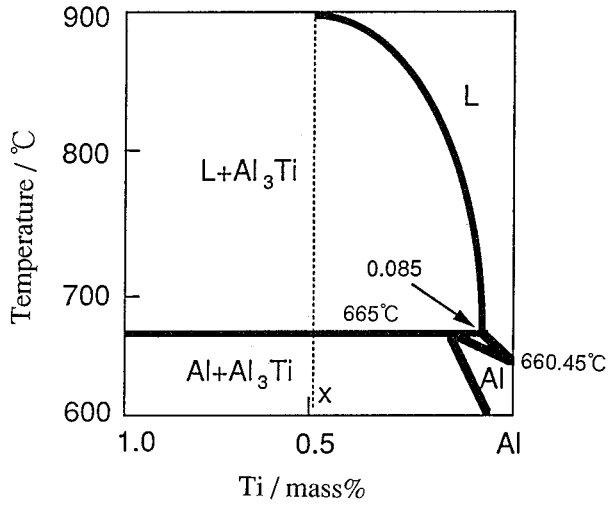

Figure 12 Al-Ti binary phase diagram around the peritectic temperature.

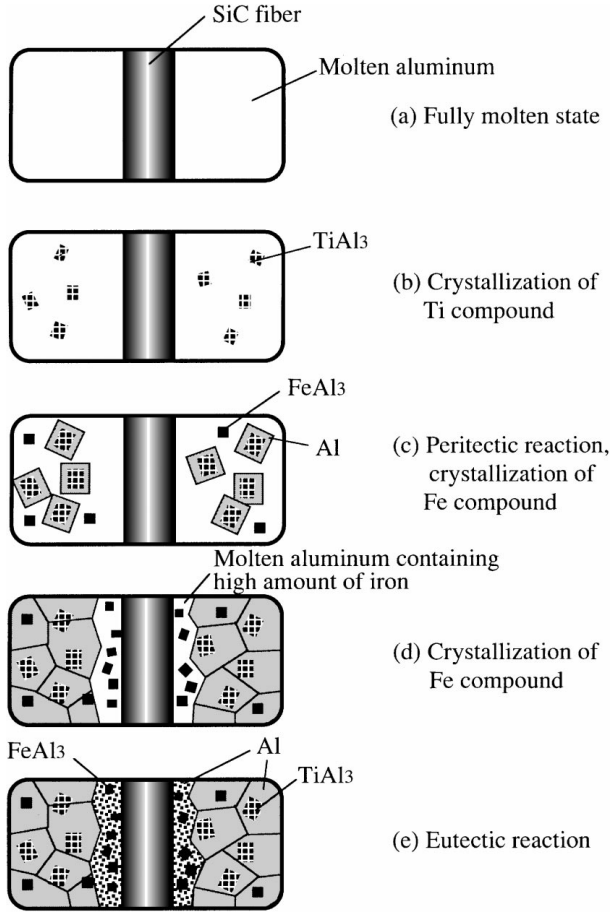

Figure 13 Solidification model of SiC/Al composite.

3.3. Radius of curvature of the composite wire at the point of interface exfoliation

The composite wire at the point of interface exfoliation during the 3 point bending tests is schematically illustrated in Fig. 9. The radius of curvature r can be determined as $r = x^2/8\delta$ by surveying x and δ in SEM photographs. The radius of curvature of the high strength elemental wire is about 75 mm.

The radius of curvature when the SiC fiber itself fractured during bending was also measured to examine the validity of the radius determined using the SEM photographs. SiC fiber was reeled onto a cylinder (radius controllable), and the radius was decreased slightly from 100 mm until the fiber broke. Mean value of the radius of curvature is 70 mm when the SiC fiber itself fractures during bending. The radius of curvature at the point of interface exfoliation is estimated from fracture distortion of SiC fiber as follows. According to data supplied in the manufacturer's catalog (Nippon Carbon Co.), the fracture distortion ε of SiC fiber is 0.014. Distance y from a neutral axis of the composite wire is approximately 1 mm. Thus the value of r can be calculated from the equation $\varepsilon = y/r$ as 70 mm, and it is in good agreement with the measured one. On the other hand, the value of δ for the low strength elemental wire is too small to survey. SiC fiber in low strength elemental wire does not demonstrate any effect from its special properties compared with the high strength elemental wire. The maximum radius of curvature at the point of interface exfoliation is about 70 mm, which means that there should be no problems with transporting and storing the wire to prevent its practical use.

3.4. Formation mechanism of Fe compound at SiC fiber/Al interface

Fig. 10 shows EPMA images of a longitudinal section around cracked areas of each composite wire. Only a small amount of Fe is detected and uniformly dispersed Ti is observed in the Al matrix for the high strength elemental wire. On the other hand, more Fe is contained in the low strength elemental wire and it is localized only at the SiC/Al interface, while Ti is still uniformly dispersed in the Al matrix. We expect that SiC and Al combine inseparably with each other due to the Fe compound. Fig. 11 shows TEM images and EDX analysis of $FeAl_3$ compound of SiC/Al interface of low strength elemental wire which confirm $FeAl_3$ is localized only on the SiC fiber surface.

This phenomenon can be understood from information contained in the Al-Ti binary phase diagram shown in Fig. 12. The solidification process of molten Al containing 0.5 mass % Ti is explained as follows using Fig. 13. Ti in molten Al is crystallized as $TiAl_3$ by a peritectic reaction (Fig. 13b), and it is completed at 665 °C (Fig. 13d). Fe in molten Al, then is crystallized as $FeAl_3$ by a eutectic reaction at 652 °C (Fig. 13e). Accordingly, the Fe impurity remains in the molten Al after Ti crystallization. Thus Ti and part of the Fe are uniformly distributed in the solidified Al matrix. The remaining Fe is crystallized as $FeAl_3$ by the eutectic reaction in the last stage of Al solidification. Thermal conductivity of SiC fiber is approximately 12 W/mK, which is much lower than that of Al, 127 W/mK. Molten Al around the SiC fiber solidifies finally, and the Fe compound is crystallized around the fiber. The Fe compound is expected to crystallize around the SiC fiber when Al contains more than 0.085 mass % Ti. Mixing of Fe impurity should be prevented.

4. Conclusions

We examined the effect of Fe impurity on mechanical properties of SiC/Al composite cable and found out the following:

1. Tensile strength of the Fe-free high strength elemental wire was 390 MPa, while tensile strength of the low strength elemental wire containing 0.36 mass % Fe was 190 MPa.

2. Pull-out of preformed wire, not its SiC fiber, took place during the 3-point bending tests based on *in situ* SEM observation of the failure process of elemental wire.

3. Unevenness at the fracture surface of high strength elemental wire was larger than that of low strength elemental wire indicating that the pull-out of fiber of high strength elemental wire was extensive.

4. From the results of *in situ* SEM observation and video tape recording of the 3-point bending tests, the destruction process of elemental wire was proposed as follows:

(a) the fiber/Al interface near the surface exfoliates;
(b) preformed wire near the surface breaks;
(c) the Al layer near the surface breaks;
(d) the preformed wire deeper than that in (b) breaks; and
(e) the Al layer deeper than that in (c) breaks.

5. In the cooling process of the molten Al containing Fe and Ti, the Ti compound crystallized uniformly in the Al matrix by a peritectic reaction, and then, $FeAl_3$ compound crystallized by a eutectic reaction. Because of the low thermal conductivity of SiC fiber, the molten Al around the SiC fiber solidified last, so that $FeAl_3$ compound was localized around the fiber.

References

1. K. OUCHI *et al*., in Proceedings of National Convention Record IEE Japan (Waseda University, Tokyo, 1996) p. 7.1.
2. J. SAWADA *et al*., in Proceedings of the Seventh Annual Conference of Power & Energy Society, IEE of Japan (Osaka University, Osaka, 1996) p. 739.
3. A. OZAWA *et al*., in Proceedings of the Annual Meeting of Japan Ceramics Society (Yokohama National University, Yokohama, 1996) p. 234.
4. Y. YASUTOMI, J. SAWADA, T. KIKUCHI, K. NAKAMURA, Y. MANABE, K. NAGANO, H. KURODA, T. SUMI, H. KUBOKAWA, M. NAGAI, H. KOGURE, Y. SAWAI and T. KISHI, submitted to *J. Mater. Sci.*
5. S. YAJIMA, K. OKAMURA, J. HAYASHI and M. OMORI, *J. Amer. Ceram. Soc.* **59** (1976) 3.
6. S. TOWATA and S. YAMADA, J. Japan Inst. Metals **47** (1983) 159.
7. Y. KAGAWA and B.-H. CHOI, *ibid.* **53** (1989) 339.
8. Y. IMAI, M. TAKEDA, H. ICHIKAWA and T. ISHIKAWA, *J. Japan Inst. Light Metals* **40** (1990) 202.
9. H. LIU, U. MADALENO, T. SHINODA, Y. MISHIMA and T. SUZUKI, *J. Mater. Sci.* **25** (1990) 4247.
10. B. J. WENG, S. T. CHANG and R. H. HO, in Proceedings of Symposium on Control of Interfaces in Metal and Ceramics Composites (San Francisco, CA, 1993) p. 197.
11. A. R. CHAPMAN, S. M. BLEAY and V. D. SCOTT, *J. Mater. Sci.* **29** (1994) 4523.
12. K. YAMADA, S. SEKIGUCHI, K. HASHIMOTO and T. ISHIDA, *J. Japan Inst. Metals* **59** (1995) 15.

Received 30 October 1997
and accepted 4 November 1998